



Process Parameter Impact on Suspension-HVOF-Sprayed Cr₂O₃ Coatings

Jarkko Kiilakoski¹ · Richard Trache² ·
Stefan Björklund³ · Shrikant Joshi³ · Petri Vuoristo¹

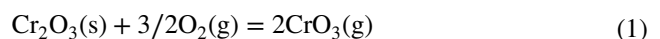
Submitted: 9 July 2019 / in revised form: 6 September 2019 / Published online: 31 October 2019
© The Author(s) 2019

Abstract Chromium oxide (Cr₂O₃) is commonly used as an atmospheric plasma-sprayed (APS) coating from powder feedstock in applications requiring resistance to sliding wear and corrosion, as well as amenability to texturing, e.g., in anilox rolls. Recently, high-velocity oxy-fuel spray methods involving suspension feedstock have been considered an extremely promising alternative to produce denser and more homogeneous chromium oxide coatings with lower as-sprayed surface roughness, higher hardness and potentially superior wear performance compared to conventional APS-sprayed coatings. In this study, the impact of process parameters namely auxiliary air cleaning nozzles and a transverse air curtain on suspension high-velocity oxy-fuel-sprayed Cr₂O₃ suspensions is presented. The produced coatings are characterized for their microstructure, mechanical properties and wear resistance by cavitation erosion. The results reveal the importance of optimized air nozzles and air curtain to achieve a vastly improved coating structure and performance.

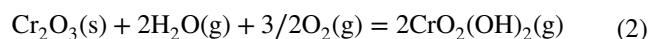
Keywords Cr₂O₃ · influence of spray parameters · mechanical properties · SHVOF · suspension spraying

Introduction

Thermally sprayed chromium oxide coatings are known to exhibit a very high hardness of up to 1900–2000 HV_{5N} (Ref 1) and possess good adhesive and abrasion wear resistance (Ref 2) in conjunction with excellent corrosion properties (Ref 3). Chromium oxide coatings are commonly used in applications such as anilox rolls and doctor blades in the paper making industry (Ref 4), pump sleeves and feeding screws (Ref 3, 5, 6) where their wear and corrosion resistance is beneficial. Chromium oxide has traditionally been processed by atmospheric plasma spray (APS) (Ref 6, 7), but other methods like high-power atmospheric plasma spray (Ref 7), detonation gun spraying (Ref 8) or HVOF spraying (Ref 9, 10) have also been explored. One of the greatest challenges in spraying Cr₂O₃ is its high volatility at high temperatures encountered during spraying, leading to formation of gaseous species according to (Ref 11–13)



in a dry atmosphere or



in a moist atmosphere. Although the above gaseous species cannot be verified from samples of thermally sprayed Cr₂O₃ coatings, Cr(VI) has been detected therein (Ref 14). The vaporization also lowers significantly the deposition efficiency (DE) and can adversely influence coating quality. To hinder vaporization, among other benefits, specific additives, such as TiO₂ or Al₂O₃, are commonly used with Cr₂O₃. (Ref 1, 15, 16) Additionally, with conventional APS processes, the reducing hydrogen-containing atmosphere can lead to further reduction of the chromia to Cr, CrO and Cr₃O₄. (Ref 5, 17) The lower temperature and a less reducing atmosphere

✉ Jarkko Kiilakoski
jarkko.kiilakoski@saint-gobain.com

¹ Materials Science and Environmental Engineering, Tampere University, Korkeakoulunkatu 6, 33720 Tampere, Finland

² Treibacher Industrie AG, Althofen, Austria

³ Production Technology, University West, Trollhättan, Sweden

of gas-fuel HVOF torches could be beneficial in removing the problem of unwanted reactions during spraying of Cr_2O_3 .

Thermal spraying with suspension feedstock is increasingly emerging as an attractive extension of the traditional thermal spray coating methods. In suspension spraying, the feedstock consists of fine particles suspended in an aqueous or organic solvent. The technique is used with both plasma and HVOF spray processes and aims to achieve finer, even nanosized microstructures, thereby altering the properties of the coating significantly. Indeed, one of the main advantages is the injection of fine particles directly into the flame, circumventing the problems of poor flowability associated with fine powder feedstock. (Ref 18–20). Suspensions have been utilized mainly for spraying materials such as TiO_2 (Ref 21–23), Cr_2O_3 (Ref 23–25), YSZ (Ref 26–28), hydroxyapatite (Ref 29, 30) and Al_2O_3 (Ref 31–34). However, the majority of suspension spraying development has focused on the improvement in YSZ coating properties, where the results have already led to the commercial application of thermal barrier coatings by suspension plasma spraying (SPS). The previous works on Cr_2O_3 suspensions have had a strong emphasis on the development of the suspensions of both pure Cr_2O_3 and its mixtures with TiO_2 . (Ref 23–25)

Currently, suspension spraying technology has matured to the point of emergence of various commercially available sources for feedstock. However, knowledge on the spraying of these feedstocks and functional performance of the resulting coatings, particularly for wear applications, is scarce and needs to be comprehensively explored. Especially in the case of Cr_2O_3 , the underlying problems of volatility and reduction reactions during spraying still exist and need to be tackled systematically in order to establish economical feasibility, technical capability and reproducibility of the process. In this study, we reveal the path of parameter screening used for optimizing S-HVOF spraying of Cr_2O_3 suspension. In the process, the impact of spray parameters varied, i.e., oxygen/fuel ratio, suspension feed rate and spray distance on coating properties is also established. Additionally, different auxiliary air cooling/cleaning systems attached to the S-HVOF spray process were evaluated to enhance the removal of unmelted fine particles during coating (Ref 1). The coatings are characterized based on their cross-sectional microstructures, Vickers microhardness and surface roughness. The best coatings from the final optimization were also subjected to cavitation erosion tests to determine their structural integrity.

Experimental Methods

Coating Deposition

The coatings were deposited on stainless steel (AISI 316) substrates with a TopGun HVOF system (GTV GmbH, Luckenbach, Germany) using ethene as the combustion gas. The spray torch was modified for liquid feedstock spraying by an in-house made injector with an internally mixing two-fluid atomizing nozzle and a conical combustion chamber, where the suspension was injected axially. Nitrogen was used as the atomizing gas for the suspension. The process parameters are presented in Table 1 and a schematic presentation of the suspension injector in Fig. 1. A commercially available suspension feedstock was used in this study (AuerCoat[®] Cr_2O_3 Suspension, Treibacher Industrie AG, Althofen, Austria). The solid content in the suspension was 40 wt.% of Cr_2O_3 (>99% purity) in water, and the size of the particles was $d_{10} = 0.2\text{--}0.8\ \mu\text{m}$, $d_{50} = 2\text{--}5\ \mu\text{m}$ and $d_{90} = 5\text{--}10\ \mu\text{m}$. The suspension was fed with an in-house made pressure-vessel-type feeder connected to a closed-loop mass flowmeter for the liquid. A suspension feed rate of up to 53 g/min was used, corresponding to a solid feed rate of 21 g/min. Flat substrate specimens grit-blasted with 180–220 mesh alumina were affixed on a plane during spraying and air cooling was utilized. The investigated parameters were as follows: spray distance, airflow through air cooling nozzles, air pressure of an air curtain, amount of suspension feed and the amount of total combustion gas flow (given in Tables 2 and 3). The substrate temperature was monitored with an infrared thermal camera (TI300, Fluke Co., Everett, WA, USA), and it was ensured that the temperature of the sample did not rise above 250 °C. A new spray pass was started when the temperature dropped to 200 °C. A pair of Silvent 209L (Silvent AB, Borås, Sweden) air cooling nozzles (“1.” in Fig. 2), one preceding and one following the spray torch,

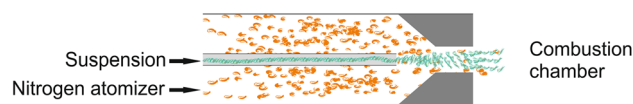


Fig. 1 A schematic illustration of the internally mixing two-fluid atomizing nozzle of the suspension injector

Table 1 Fixed process parameters during process parameter impact studies

Chamber type, mm	Suspension injector diameter, mm	Ethene flow, slpm	Oxygen flow, slpm	Step, mm	Surface speed, m/min	Atomizer gas, slpm
135, conical	0.8	88	213	3	57	4.5

Table 2 Summary of varied process parameters and corresponding hardness and roughness results

Parameter	Susp. Feed, g/min	Spray distance, mm	Passes	Flow rate of air nozzles, slpm	Pass thickness, $\mu\text{m}/\text{pass}$	Hardness [HV _{0.3}]	S_a , μm
H-110-0-0	53	110	20	...	5	957 ± 60	2.5
H-100-0-0	53	100	20	...	4	1060 ± 45	2.2
H-90-0-0	53	90	20	...	5	1141 ± 106	4.0
H-80-0-0	53	80	20	...	5	1396 ± 132	7.3
H-80-400-0	50	80	20	400	6	1416 ± 67	2.9
H-90-400-0	50	90	20	400	6	1368 ± 143	1.3
H-80-600-0	50	80	20	600	7	752 ± 91	14.0
H-90-600-0	50	90	20	600	5	1380 ± 23	3.8
L-80-600-0	23	80	12	600	2	1444 ± 57 HV _{0.05}	3.6
L-90-600-0	23	90	12	600	2	903 ± 391 HV _{0.05}	3.0

Specimen nomenclature specifies suspension feed: H/L (High/Low)-spray distance–air nozzle flow–air curtain pressure

Table 3 Summary of varied process parameters used with the evaluation of the transverse air curtain and corresponding hardness and roughness results

Parameter	Ethene flow, slpm	Oxygen flow, slpm	Susp. Feed, g/min	SD, mm	Passes	Pass thickness, $\mu\text{m}/\text{pass}$	Air curtain pressure, MPa	Hardness [HV _{0.3}]	S_a , μm
H-90-400-2	88	213	47	90	20	6	0.2	1358 ± 44	3.4
H-90-400-4	88	213	50	90	20	6	0.4	1351 ± 47	1.9
H-90-400-7	88	213	50	90	20	6	0.7	1495 ± 71	1.8
H-90-400-7 (g)	120	275	40	90	20	4	0.7	1335 ± 66	2.4
L-90-400-4	88	213	20	90	40	2	0.4	1277 ± 88	1.8

Specimen nomenclature specifies suspension feed: H/L (High/Low)-spray distance–air nozzle flow—transverse air curtain pressure, (g) = alternate gas parameters

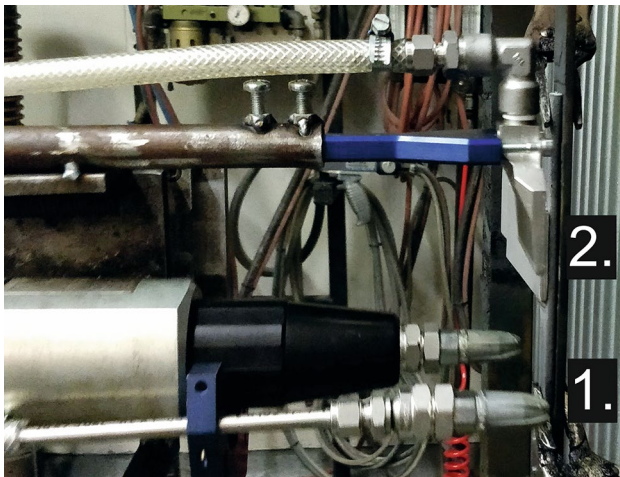


Fig. 2 Auxiliary cooling systems utilized in the study. 1. Air nozzles parallel to the spray plume. 2. Air curtain transverse to the spray plume

were used, and a Silvent 973 air curtain nozzle (“2.” in Fig. 2) was also transversely mounted at a distance of about 70 mm from the nozzle exit.

Coating Characterization

The coating cross sections were characterized with a scanning electron microscope (SEM) (IT500, JEOL Ltd., Tokyo, Japan) with a 15 kV accelerating voltage, and the cross-sectional microhardness values were averaged from five indentations made with a Vickers microhardness tester (MMT-X7, Matsuzawa Co., Ltd., Akita, Japan) at a load of 300 grams. Surface roughness values (S_a) of the specimens were measured with an InfiniteFocus G5 (Alicona Imaging GmbH, Austria) optical profilometer over an area profile of $1.62 \times 1.62 \text{ mm}^2$. Cavitation erosion tests were performed with an ultrasonic transducer (VCX-750, Sonics and Materials Inc., Newtown, CT, USA), according to the ASTM G32-10 standard for indirect cavitation erosion. The vibration tip, made of a Ti-6Al-4 V alloy, was placed at a distance of 0.5 mm from the sample surface and vibrated at a frequency of 20 kHz with an amplitude of 50 μm . The coated samples were cleaned in an ultrasonic bath with ethanol and weighed after drying. Samples were periodically weighed after 15, 30, 60 and 90 min of testing. The sample surfaces were tested as-sprayed. The length of the cavitation test

along with the periodic intermittent weight measurements increases the statistical validity of the test, and, hence, only one sample per coating was tested. The mean depth of erosion (MDE) was calculated following the equation

$$\text{MDE} \left[\frac{\mu\text{m}}{\text{min}} \right] = \frac{1000 \left[\frac{\mu\text{m}}{\text{m}} \right] * \text{SER} \left[\frac{\text{mm}^3}{\text{h}} \right]}{60 \left[\frac{\text{min}}{\text{h}} \right] * A [\text{mm}^2]},$$

where SER is the volume loss per hour calculated from the last three measuring points (1 h) to remove the effects of the bubble incubation stage and surface roughness and A is the surface area of the vibrating tip. The coatings were presumed to be fully dense Cr_2O_3 when volume loss was calculated from mass loss for simplicity. Cavitation resistance of the coatings was then calculated as the reciprocal of the mean depth of erosion.

Results and Discussion

Influence of Spray Distance

The starting parameters for the initial investigation of the coatings originated from our previous experience with liquid feedstock HVOF spraying and from the spray parameters used by Toma et al. (Ref 23). The parameters are presented in

Table 1. To assess the role of gun-to-substrate standoff distance on coating quality, specimens were first sprayed at four spray distances of 80, 90, 100 and 110 mm. From the cross sections of the resulting set of coatings shown in Fig. 3, it is evident that all the coatings have visible interfaces between successive spray passes, which could be attributable to the presence of some microporosity, dust or vaporized and condensed Cr_2O_3 . This is likely to diminish the structural integrity of the coating. All the coatings also exhibited cracking, either in the vertical or horizontal directions or both, suggesting excessive thermal loading from the relatively short spray distance. Regardless, the coating hardness values measured in the range 950–1400 HV_{0.3} were comparable to the value of 1400 HV_{0.3} obtained by Toma et al. (Ref 23). The deposition rates were also reasonable at roughly 5 μm per pass, which is consistent with our experience with HVOF spraying of Cr_2O_3 powders. The as-deposited coating surfaces were found to be increasingly uneven (higher S_d) when moving to shorter spray distances, as seen in the surface morphology images in Fig. 3 and also quantified by the roughness values in Table 2. This phenomenon is speculated to arise from the higher surface temperature trapping more fine particles that are not directly deposited,

but are traveling perpendicular to the surface away from the torch, as explained in detail by VanEvery et al. (Ref 27) and Fauchais et al. (Ref 1). This leads to greater deposition on surface asperities of the substrate for shorter spray distances. As a suitable compromise between hardness and roughness, spray distances of 80 and 90 mm were chosen for the ensuing parametric studies. Additionally, it became clear that cleaning the surface of unmelted/condensated fine chromia particles between the coating layers could be beneficial in reducing interpass porosity. Therefore, air nozzles were mounted on both sides of the torch (see arrangement 1 in Fig. 2).

Influence of the Airflow of Air Cooling Nozzles

The flow in the air nozzles could be adjusted between 0 and 600 slpm with an accuracy of 50 slpm. By manually determining flow rates that would be high enough without apparently interfering with the spray plume, the flow rates to be investigated were chosen to be 400 and 600 slpm. Apart from the spray distances of 80 and 90 mm chosen based on the preceding set of experiments, only the suspension feed was varied for a couple of runs, roughly halving it to 23 g/min to assess the corresponding influence on coating quality. In all the coatings, there was still fine particulate dust visible at the spray pass interfaces, as seen in the exemplary cross-sectional micrographs from coatings in Fig. 4. Some horizontal and treelike cracks were seen in the coatings at the spray distance of 80 mm (see Fig. 4c), regardless of the airflow in the nozzles. This suggests that 90 mm is the more suitable spray distance, as it keeps the temperature of the substrate/coating system better under control with milder heat cycling. In particular, H-90-400-0 and H-90-600-0 exhibited no cracking and their cross sections seemed quite coherent. The hardness of both coatings was around 1350–1400 HV_{0.3}. It is also evident that 600 slpm airflow is excessive with 80 mm spray distance (coating H-80-600-0), as the airflow appears to promote column formation by the fine particles (Fig. 5c, left), due to the higher airflow promoting deviation of the trajectory of the still molten fines, leading to a slightly cauliflower-like surface structure often associated with a columnar structure (Ref 27). This apparently increases the measured pass thickness and, coupled with crack formation from the dissimilar thermal history of the coating layers, leads to subpar hardness of less than 800 HV_{0.3} (as compared to the ca. 1400 HV_{0.3} for H-80-0-0 and H-80-400-0). The additional 10 mm distance between the air nozzles and the substrate seems to make a significant difference between H-80-600-0 and H-90-600-0, as is evident from Figs. 4c and 5c.

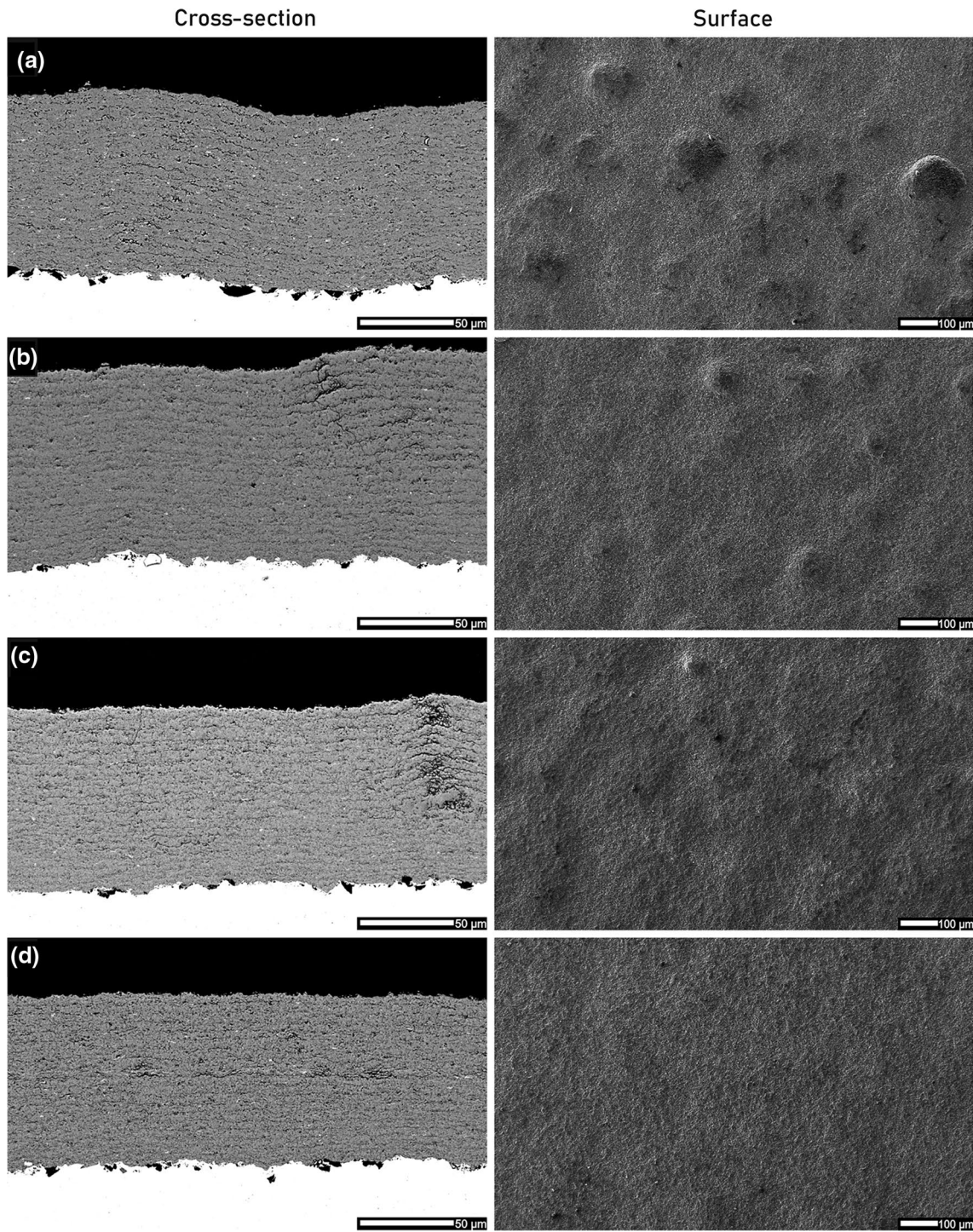


Fig. 3 SEM (SE) images of the cross sections and surface morphologies of coatings deposited with varying spraying distance: (a) 80 mm (H-80-0-0), (b) 90 mm (H-90-0-0), (c) 100 mm (H-100-0-0), (d) 110 mm (H 110-0-0)

Influence of the Suspension Feed Rate

One set of experiments involved keeping the 600 slpm air nozzle flow rate, but reducing the suspension feed rate by approximately a factor of two (to 23 g/min, coatings

L-80/90-600-0). As expected, the corresponding deposition rate dropped to 2 μm/pass. Although these coating runs were interrupted, they clearly revealed that the longer spray distance of 90 mm led to a significant drop in hardness while at a spray distance of 80 mm the coating exhibited promising

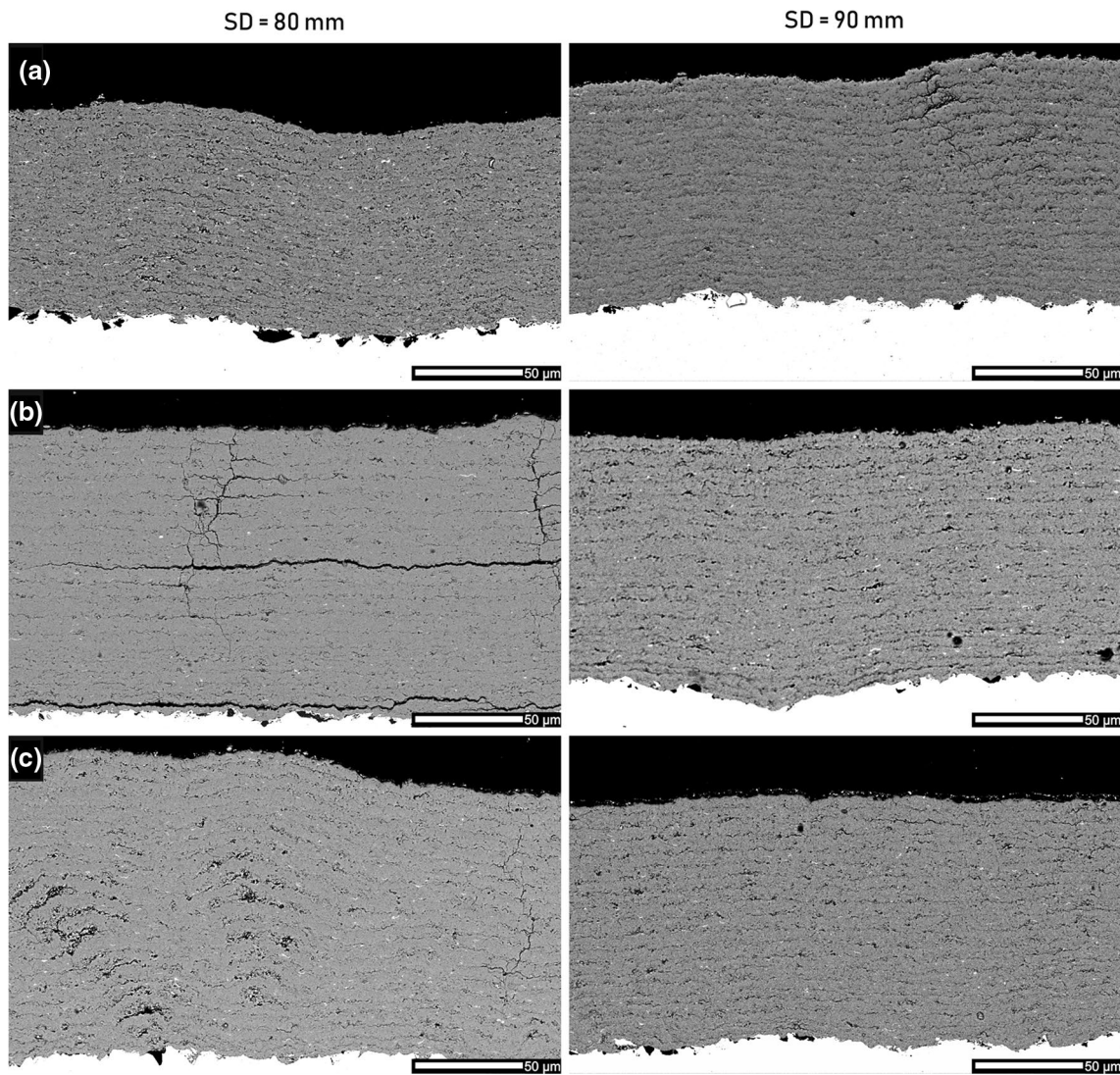


Fig. 4 Cross-sectional SEM (SE) images of microstructures of coatings showing the evolution in structure when an air cooling nozzle was used: (a) 0 slpm (H-80/90-0-0), (b) 400 slpm (H-80/90-400-0), (c) 600 slpm (H-80/90-600-0)

hardness. This difference could possibly be attributed to higher degree of atomization of the suspension followed by a more pronounced scattering of droplets in the flame when compared to the higher feed rate. This would lead to the smaller droplets losing their momentum with the longer spray distance combined with the strong stagnation zone from the air nozzle flow. Due to the inconclusive results, the lower feed rate was decided to be also investigated in the following step while maintaining the flow rate through the air nozzle at 400 slpm.

Influence of the Air Pressure, the Transverse Air Curtain and Fuel Gas Flow

The pressure for the air curtain was chosen to be 0.2, 0.4 and 0.7 MPa to facilitate removal of fine particles without

affecting melting of the particles excessively. Even with 0.2 MPa of transverse air curtain pressure, an improvement was seen in the coating microstructure as less pronounced interpass porosity and a more homogeneous surface topography, which is shown in Fig. 6.

With increasing air curtain pressure, the surface roughness of the coatings was generally found to be lower while the hardness values remained the same or slightly increased, as given in Table 3. At the same time, the thickness per pass was essentially unaltered. The beneficial effect of the air curtain was seemingly achieved with 0.4 MPa pressure, as can be seen in the images for SD = 90 mm in Fig. 6. It is pertinent to note that the surface and cross-section images do not show additional improvement when the pressure was further increased from 0.4 to 0.7 MPa. The surface roughness did not improve either when the air curtain pressure

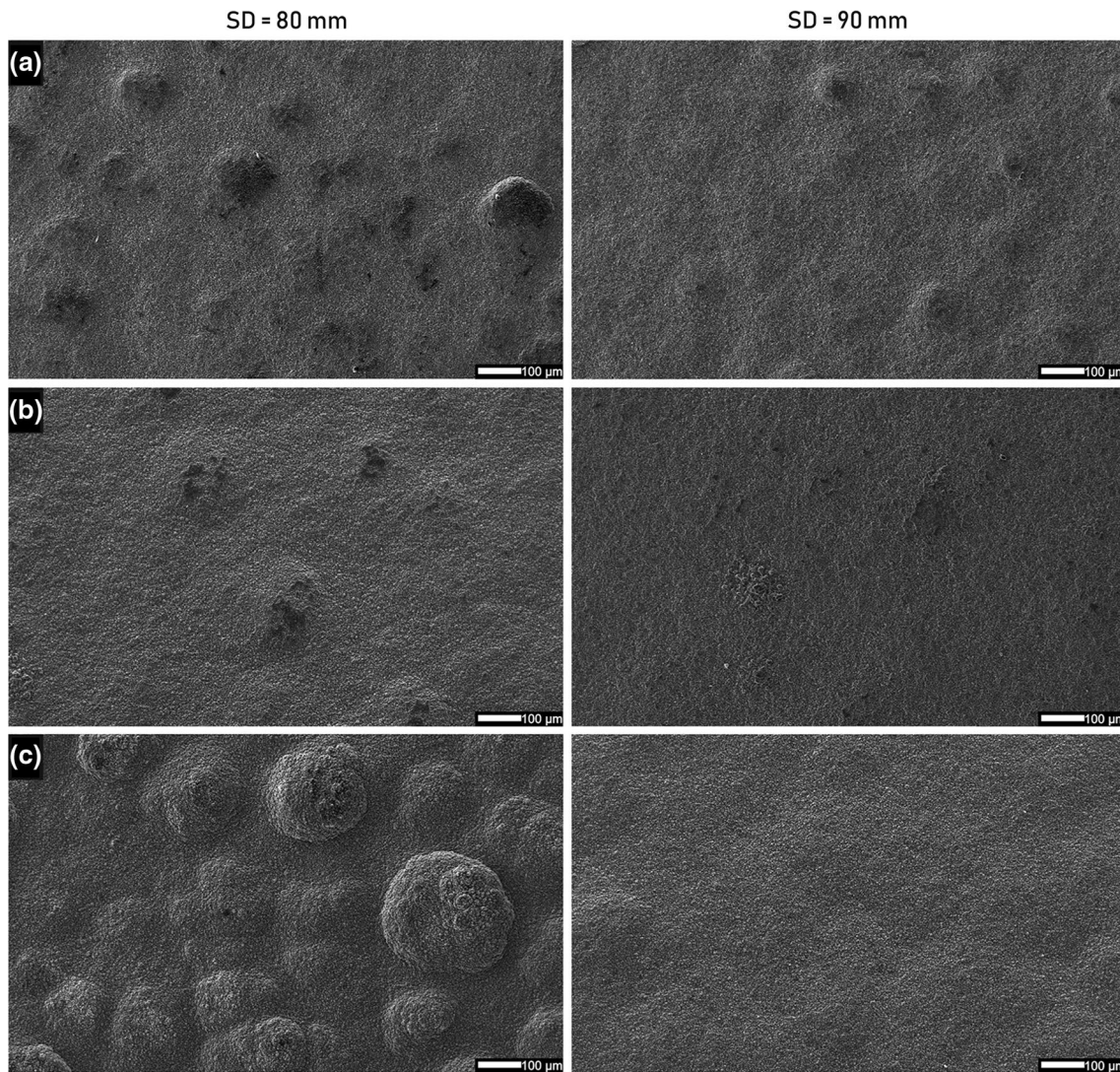


Fig. 5 Surface morphology SEM (SE) images of microstructures of coatings showing the evolution in structure when an air cooling nozzle was used: (a) 0 slpm (H-80/90-0-0), (b) 400 slpm (H-80/90-400-0), (c) 600 slpm (H-80/90-600-0)

was increased from 0.4 to 0.7 MPa. Therefore, an air curtain pressure of 0.4 MPa was used to investigate the effect of a lower feed rate of 20 g/min (coating L-90-400-4), which led to the deposition rate being halved while the hardness lowered slightly and the roughness remained the same.

The higher air curtain pressure of 0.7 MPa was chosen when evaluating the effect of higher gas flow of the fuel and oxygen in H-90-400-7(g). The choice was made to ensure that the curtain is powerful enough even with the increased density of the flame of the torch. The increased flame velocity led to a lower deposition rate, through a combination of a lower suspension feed and likely either less melting of the feedstock due to the shorter dwell time or a reduction in the velocity of the particles prior to impact due to a stronger stagnation zone close to the surface. This stagnation can lead to a reduction in

perpendicular velocity for small particles to almost zero, while the radial velocity can reach 100 m/s (Ref 35), easily leading to off-normal impact and consequent deposition of the particles. (Ref 36) The shorter dwell time may be insufficient time to melt the particle thoroughly, even though the higher total gas flow often leads to an increase in particle temperature. (Ref 37) However, the temperature is always measured from the surface of the particle, and the convection and conduction of the heat inside the particle takes time. (Ref 38) An increase of 80 slpm, in an example of a DJ-2600 Hybrid, of gas flow would increase the particle velocity by 70 m/s and its temperature by 30 °C. (Ref 37) Therefore, it is likely that the reduction in the dwell time has more influence than the increase in temperature.

The hardness was lower and the roughness higher when compared with H-90-400-7.

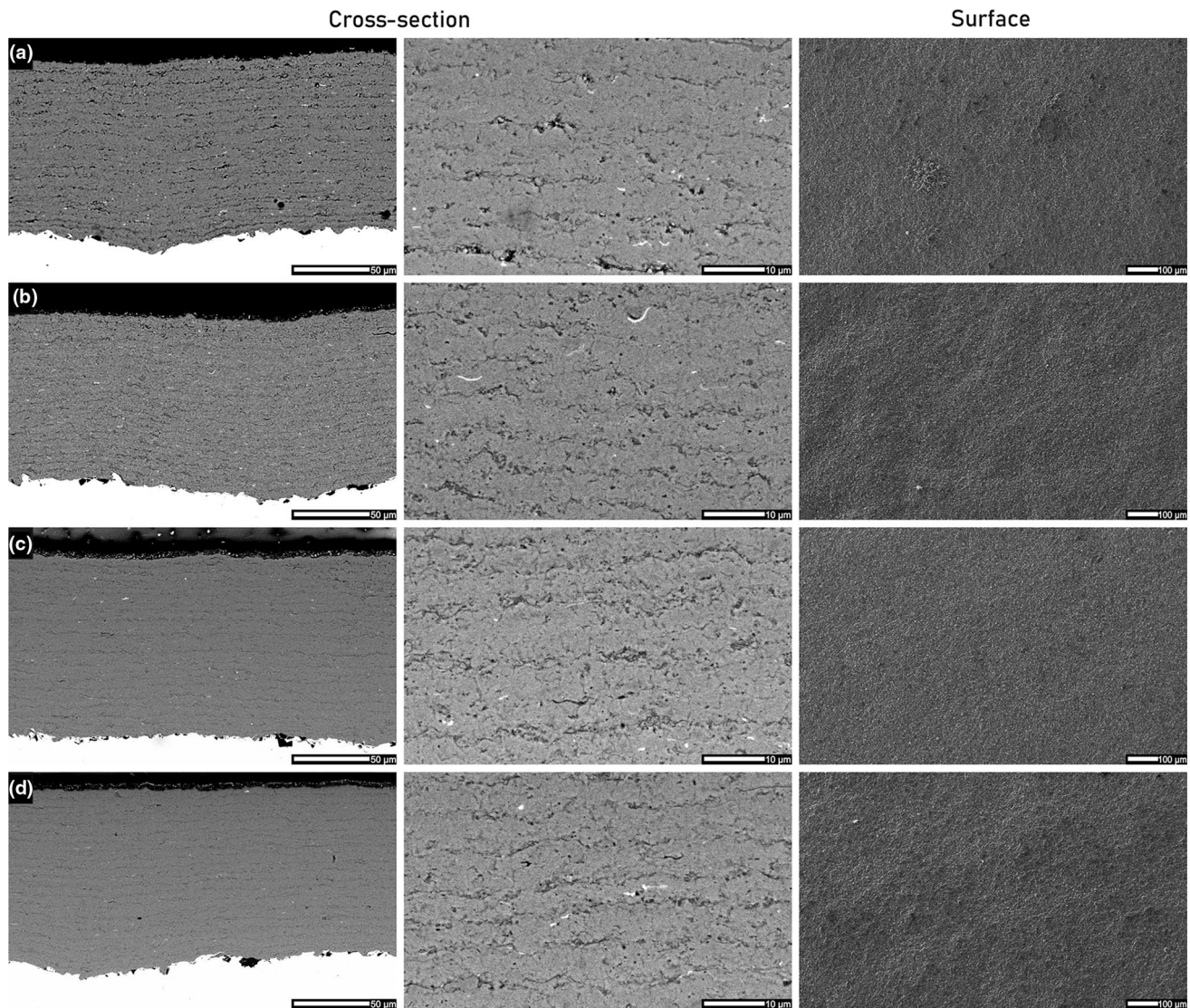


Fig. 6 Cross-sectional SEM (SE) images of microstructures of coatings with $SD=90$ showcasing the effect of transverse air curtain pressure: (a) 0 bar (H-90-400-0), (b) 2 bar (H-90-400-2), (c) 4 bar (H-90-400-4), (d) 7 bar (H-90-400-7)

Physical Characterization of the Coatings

Microhardness and Roughness

The hardness and as-sprayed roughness values of all the coatings are summarized in Fig. 7. It can be said that, generally, the hardness of the coating increases with shortening of spray distance, while the roughness increases. The addition of the air nozzles improved one or both of these properties while increasing the reliability and homogeneity with the exception of H-80-600-0, where the airflow was seemingly causing too much turbulence at this short spray distance.

By addition of a transverse air curtain, the coating structure was found to become more homogeneous, eliminating the variability in hardness values of the coatings already

with a 0.2 MPa curtain pressure (coating H-90-400-2). This would indicate effective removal of fine particles that end up as defects in the coating, thereby compromising the structure. At 0.4 and 0.7 MPa transverse air curtain pressure, both the hardness variability and surface roughness were improved. Higher combustion gas flow led to slightly lower hardness and higher roughness as did the lower feed rate of suspension.

Integrity and Cohesion of Coatings as Studied by Cavitation Erosion

In the final stage of the study, the cohesion of the coatings in the H-90 series of spray runs was evaluated by cavitation erosion experiments. The coatings deposited with a spray

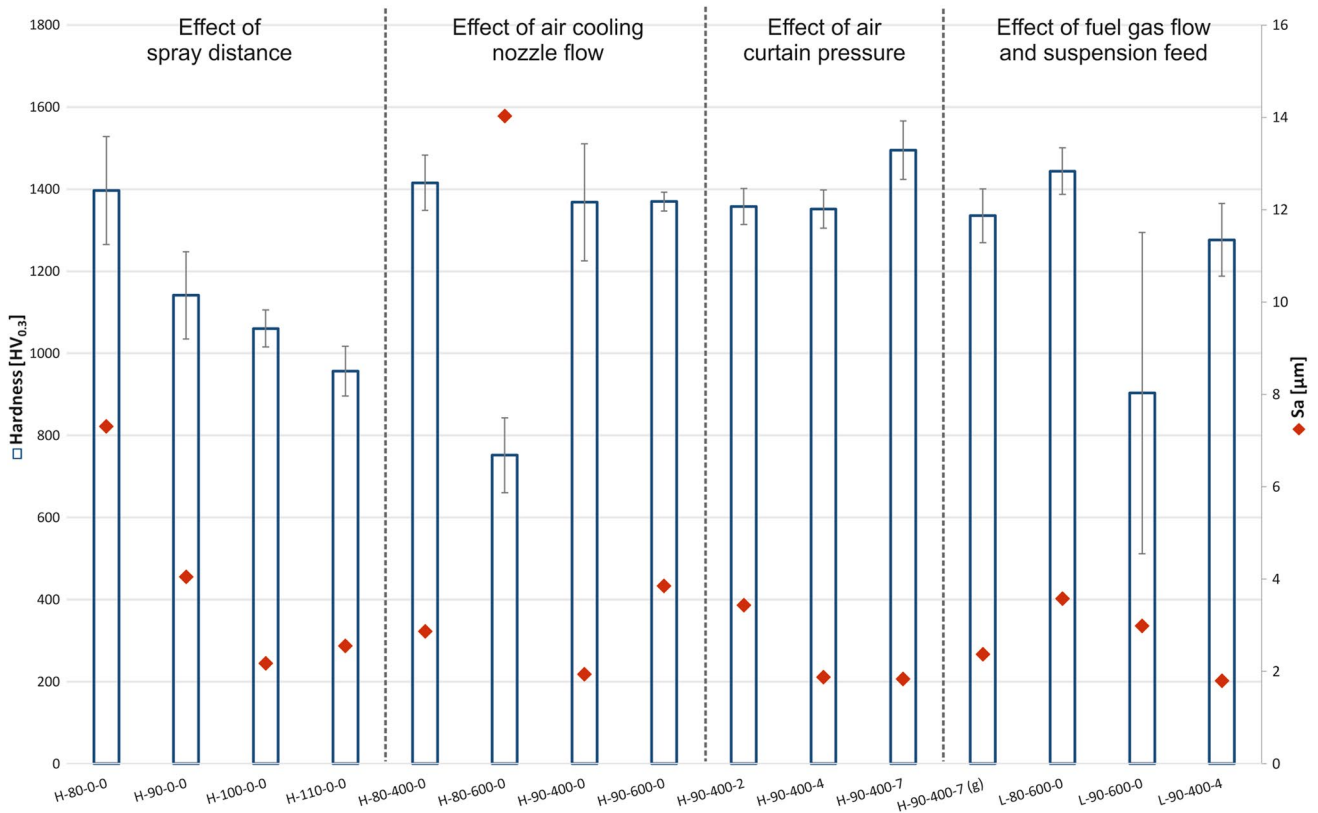


Fig. 7 Vickers hardness with its standard deviation and roughness values of all investigated coatings

distance of 90 mm were selected from previous examinations based on the *prima facie* promising overall quality of coatings (microstructure, hardness and surface roughness). Past studies have shown that cavitation erosion is a good indicator of the structural cohesion of a ceramic coating and the cavitation erosion resistance is hindered by poor splat-to-splat adherence (Ref 39, 40). This makes it ideal for testing the effect of fine particle removal from splat boundaries. The results from the cavitation erosion tests are presented in Fig. 8.

It is seen that the use of an air curtain with moderate pressures is advisable: with 0.2 and 0.4 MPa air curtain pressure, the cavitation resistance is increased, indicating improved cohesion likely due to a lower amount of poorly bonded fine particles at the splat boundaries. Increasing the air curtain pressure to 0.7 MPa decreased the cavitation resistance slightly, probably due to a decrease in the particle velocities and temperature leading to less impact energy and bonding between splats. Interestingly, higher combustion gas flows that would normally increase bonding, led to even less cohesion of the coating. This derives possibly from an increase in the amount of defects, which the higher surface roughness would indicate as well. Surface images of H-90-400-7 and H-90-400-7(g) are presented in Fig. 9 before (a) and after cavitation erosion (b). In the as-sprayed surfaces, no clear

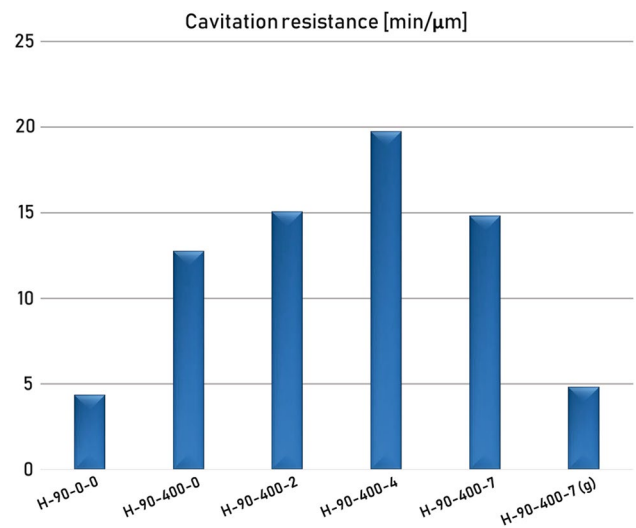


Fig. 8 Cavitation erosion resistance of coatings with 90 mm spray distance and 400 slpm air nozzle flow

difference in the amount of dust or unmelted particles can be seen. However, in H-90-400-7(g), a larger amount of protrusions are found—such as pointed by the white arrow—that likely cause the higher surface roughness. These, in unison with weak splat interfaces, provide low-energy pathways

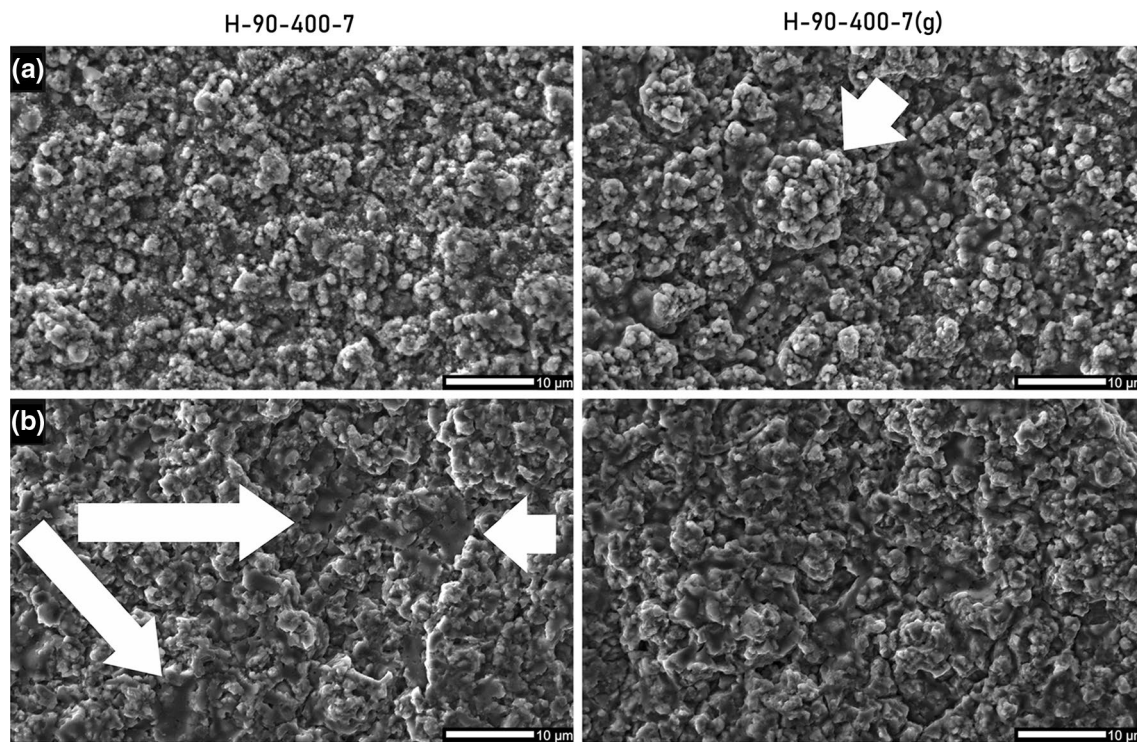


Fig. 9 Surface images (SEM) of coating H-90-400-7 and H-90-400-7(g) (a) as-sprayed and (b) after cavitation erosion. White arrows point to a protrusion in H-90-400-7(g) in (a) and to well-melted splats in H-90-400-7 revealed by cavitation erosion in (b)

to crack propagation in the coating. (Ref 41) Indeed, in Fig. 9b), large areas of well-melted splats can be seen in H-90-400-7 (white arrows), while such regions are sparse in H-90-400-7(g). This lends credibility to the idea of cooling/slowing of the particles during spraying, leading to less cohesion and a lower melting degree. It is believed that the majority cause of the weakening of the structure is due to the formation of the more pronounced stagnation zone due to the short spray distance, which affect the trajectory and velocity of the particles (Ref 36), and in a smaller part unmelted particles.

Conclusions

In this study, the effect of process parameters during SHVOF spraying of a Cr_2O_3 suspension on coating quality was investigated. The evaluated parameters were as follows: spray distance, flow rate of auxiliary air cooling nozzles for surface cleaning, pressure of a transverse air curtain for the removal of fine particles and excess heat load, total combustion gas flow and suspension feed rate. Other parameters were kept constant. All coatings were deposited with good efficiency, but the quality varied drastically. The need for auxiliary systems became clear, as fine unmelted particles were deposited on the splat interfaces, i.e., between passes of the torch. The

coatings were evaluated by their microstructure, hardness, surface roughness and cavitation erosion resistance.

The conclusions can be summarized based on the parameters as follows:

- *Spray distance* While a longer spray distance produced a smoother, cleaner coating, the hardness values were superior with shorter spray distances. A distance of 90 mm was found to be optimal.
- *Air cooling nozzles* The benefit of the surface cleaning effect of the nozzles was clear in improving the coating cohesion. However, too much airflow could cause too much turbulence at the surface, leading to higher surface roughness and lower hardness. An airflow of 400 slpm was sufficient in this study.
- *Air curtain* An improvement was seen immediately with even the lightest air curtain pressure of 0.2 MPa, visibly reducing the amount of defects between spray passes. The reduction in heat load on the samples also reduced the roughness of the coatings. While all pressure levels improved the coating, the optimal structure and cavitation erosion resistance were found with 0.4 MPa.
- *Fuel gas flow* The higher fuel gas flow led to a stronger stagnation zone close to the sample surface, decreasing the velocity and deflecting the trajectory of the particles which decreased the hardness and cavitation resistance

and increased the surface roughness. Additionally, the shorter dwell time led to less melting of the particles, causing a lower deposition rate.

- **Suspension feed rate** Lowering of the suspension feed rate by half did not bring about any improvements in the coating structure, but led to a reduction in deposition rate.

The optimization path in this work gives encouragement in the development of high-performance oxide coatings from suspension feedstock. After optimization, the coatings have good mechanical properties with a decent deposition rate, with still room to improve. Further studies should be directed toward optimizing the amount of suspension feed as well as gas flow parameters of the torch, along with different combustion chamber geometries and the effect of air curtain pressure on particle velocity, temperature and trajectory.

Acknowledgments The authors gratefully acknowledge the financial support from ‘the graduate school of the President of Tampere University of Technology’, the ‘K.F. and Maria Dunderberg Foundation’ and Business Finland (Finnish innovation funding, trade, investment and travel promotion organization), its ‘‘Ductile and Damage Tolerant Ceramic Coatings’’ project and the participating companies. The authors would like to thank Mr. Anssi Metsähonkala of Tampere University for manufacturing the coatings.

Open Access This article is distributed under the terms of the Creative Commons Attribution 4.0 International License (<http://creativecommons.org/licenses/by/4.0/>), which permits unrestricted use, distribution, and reproduction in any medium, provided you give appropriate credit to the original author(s) and the source, provide a link to the Creative Commons license, and indicate if changes were made.

References

1. P.L. Fauchais, J.V.R. Heberlein, and M.I. Boulos, Overview of Thermal Spray, *Thermal Spray Fundamentals: From Powder to Part*, P.L. Fauchais, J.V. Heberlein, and M.I. Boulos, Ed., Springer, New York, 2014, p 17-72
2. S. Usmani and K.N. Tandon, Evaluation of Thermally Sprayed Coatings under Reciprocating Lubricated Wear Conditions, *J. Therm. Spray Technol.*, 1992, **1**(3), p 249-255
3. P. Vuoristo, Thermal Spray Coating Processing, *Comprehensive Materials Processing Volume 4: Films and Coatings: Technology and Recent Development*, 1st ed., S. Hashmi, Ed., Elsevier, Oxford, 2014, p 229-276
4. J.R. Davis, ASM Handbook, Volume 5A: Thermal Spray Technology. in R.C.J. Tucker ed., (Materials Park, OH, USA), ASM International, 2013.
5. L. Pawlowski, Technology of Thermally Sprayed Anilox Rolls: State of Art, Problems, and Perspectives, *J. Therm. Spray Technol.*, 1996, **5**(3), p 317-334
6. F. Rastegar and A.E. Craft, Piston Ring Coatings for High Horsepower Diesel Engines, *Surf. Coatings Technol.*, 1993, **61**(1–3), p 36-42
7. T. Morishita, Coatings by 250 kW Plasma Jet Spray System. in *Proceedings of the 2nd Plasma Technik Symposium*, ed. by S. Blum-Sandmeier, H. Eschnauer, P. Huber, and A. Nicoll, Eds., (Luzern, Switzerland), Plasma Technik AG, Wohlen, 1992, pp. 137–142.
8. K. Niemi, P. Vuoristo, and T. Mäntylä, Chromium Oxide Coatings Deposited by Plasma Spraying and Detonation Gun Spraying. in *Proceedings of the 2nd Plasma Technik Symposium*, ed. by S. Blum-Sandmeier, H. Eschnauer, P. Huber, and A. Nicoll, Eds., (Luzern, Switzerland), Plasma Technik AG, Wohlen, 1991, pp. 311–322.
9. G. Bolelli, L. Lusvardi, T. Manfredini, F. Pighetti Mantini, R. Polini, E. Turunen, T. Varis, and S.-P. Hannula, Comparison Between Plasma- and HVOF-Sprayed Ceramic Coatings: Part I. : Microstructure and Mechanical Properties, *Int. J. Surf. Sci. Eng.*, 2007, **1**(1), p 38-61
10. T. Varis, J. Knuutila, T. Suhonen, U. Kanerva, J. Silvonen, J. Leivo, and E. Turunen, Improving the Properties of HVOF-Sprayed Cr₂O₃ by Nanocomposite Powders, *Thermal Spray 2008: Crossing Borders, on CD-ROM*, E. Lugscheider, Ed., DVS-Verlag GmbH, Düsseldorf, 2008, p 452-455
11. N. Jacobson, D. Myers, E. Opila, and E. Copland, Interactions of Water Vapor with Oxides at Elevated Temperatures, *J. Phys. Chem. Solids*, 2005, **66**(2–4), p 471-478
12. D. Caplan and M. Cohen, The Volatilization of Chromium Oxide, *J. Electrochem. Soc.*, 1961, **108**(5), p 438-442
13. G.R. Holcomb, Calculation of Reactive-Evaporation Rates of Chromia, *Oxid. Met.*, 2008, **69**(3–4), p 163-180
14. M. Harju, M. Järn, P. Dahlsten, J.P. Nikkanen, J.B. Rosenholm, and T. Mäntylä, Influence of Long-Term Aqueous Exposure on Surface Properties of Plasma-Sprayed Oxides Cr₂O₃ and Cr₂O₃-25 Wt.% TiO₂, *J. Colloid Interface Sci.*, 2008, **326**(2), p 403-410
15. L.-M. Berger, F.-L. Toma, S. Scheitz, R. Trache, and T. Börner, Thermisch Gespritzte Schichten Im System Al₂O₃-Cr₂O₃-TiO₂—Ein Update, *Materwiss. Werksttech.*, 2014, **45**(6), p 465-475
16. S.H. Yu and H. Wallar, Chromia Spray Powders. (United States), United States Patent and Trademark Office, 2006, p. 5.
17. M. Vippola, J. Vuorinen, P. Vuoristo, T. Lepistö, and T. Mäntylä, Thermal Analysis of Plasma Sprayed Oxide Coatings Sealed with Aluminium Phosphate, *J. Eur. Ceram. Soc.*, 2002, **22**(12), p 1937-1946
18. F.-L. Toma, A. Potthoff, L.-M. Berger, and C. Leyens, Demands, Potentials, and Economic Aspects of Thermal Spraying with Suspensions: A Critical Review, *J. Therm. Spray Technol.*, 2015, **24**(7), p 1143-1152
19. P. Fauchais, M. Vardelle, A. Vardelle, and S. Goutier, What Do We Know, What Are the Current Limitations of Suspension Plasma Spraying?, *J. Therm. Spray Technol.*, 2015, **24**(7), p 1120-1129
20. A. Killinger, P. Müller, and R. Gadow, What Do We Know, What Are the Current Limitations of Suspension HVOF Spraying?, *J. Therm. Spray Technol.*, 2015, **24**(7), p 1130-1142
21. G. Bolelli, V. Cannillo, L. Lusvardi, and R. Gadow, Deposition of TiO₂ Coatings: Comparison Between High Velocity Suspension Flame Spraying (HVSFS), Atmospheric Plasma Spraying and HVOF-Spraying, *Thermal Spray 2009: Expanding Thermal Spray Performance to New Markets and Applications*, B.R. Marple, M.M. Hyland, Y.-C. Lau, C.-J. Li, R.S. Lima, and G. Montavon, Ed., Springer, Las Vegas, 2010, p 207-212
22. F.-L. Toma, L.-M. Berger, I. Shakhverdova, B. Leupolt, A. Potthoff, K. Oelschlägel, T. Meissner, J.A.I. Gomez, and Y. de Miguel, Parameters Influencing the Photocatalytic Activity of Suspension-Sprayed TiO₂ Coatings, *J. Therm. Spray Technol.*, 2014, **23**(7), p 1037-1053
23. F.L. Toma, A. Potthoff, and M. Barbosa, Microstructural Characteristics and Performances of Cr₂O₃ and Cr₂O₃-15%TiO₂ S-HVOF Coatings Obtained from Water-Based Suspensions, *J. Therm. Spray Technol.*, 2018, **27**(3), p 344-357

24. R. Gadow, A. Killinger, and J. Rauch, New Results in High Velocity Suspension Flame Spraying (HVSFS), *Surf. Coat. Technol.*, 2008, **202**(18), p 4329-4336
25. J. Rauch, G. Bolelli, A. Killinger, R. Gadow, V. Cannillo, and L. Lusvardi, Advances in High Velocity Suspension Flame Spraying (HVSFS), *Surf. Coat. Technol.*, 2009, **203**(15), p 2131-2138
26. A. Killinger, M. Kuhn, and R. Gadow, High-Velocity Suspension Flame Spraying (HVSFS), A New Approach for Spraying Nanoparticles with Hypersonic Speed, *Surf. Coat. Technol.*, 2006, **201**(5), p 1922-1929
27. K. VanEvery, M.J.M. Krane, R.W. Trice, H. Wang, W. Porter, M. Besser, D. Sordelet, J. Ilavsky, and J. Almer, Column Formation in Suspension Plasma-Sprayed Coatings and Resultant Thermal Properties, *J. Therm. Spray Technol.*, 2011, **20**(4), p 817-828
28. M. Marr, J. Kuhn, C. Metcalfe, J. Harris, and O. Kesler, Electrochemical Performance of Solid Oxide Fuel Cells Having Electrolytes Made by Suspension and Solution Precursor Plasma Spraying, *J. Power Sour.*, 2014, **245**, p 398-405
29. N. Stiegler, D. Bellucci, G. Bolelli, V. Cannillo, R. Gadow, A. Killinger, L. Lusvardi, and A. Sola, High-Velocity Suspension Flame Sprayed (HVSFS) Hydroxyapatite Coatings for Biomedical Applications, *J. Therm. Spray Technol.*, 2012, **21**(2), p 275-287
30. G. Bolelli, D. Bellucci, V. Cannillo, R. Gadow, A. Killinger, L. Lusvardi, P. Müller, and A. Sola, Comparison between Suspension Plasma Sprayed and High Velocity Suspension Flame Sprayed Bioactive Coatings, *Surf. Coat. Technol.*, 2015, **280**, p 232-249
31. J. Kiilakoski, A. Lutoschkin, M. Plachetta, M. Apostol, H. Koivuluoto, P. Müller, A. Killinger, P. Vuoristo, Fracture Characteristics of High-Velocity Suspension Flame-Sprayed Aluminum Oxide Coatings. in *Proceedings of the International Thermal Spray Conference*, (May 10–12, 2016 (Shanghai, China)), DVS Media GmbH, Düsseldorf, Germany, 2016, pp. 466–471.
32. F.-L. Toma, S. Langner, M.M. Barbosa, L. Berger, C. Rödel, A. Potthoff, Influence of the Suspension Characteristics and Spraying Parameters on the Properties of Dense Suspension-HVOF Sprayed Al₂O₃ Coatings. in *Thermal Spray 2011: Proceedings of the International Thermal Spray Conference*, ed. by B.R. Marple, A. Agarwal, M.M. Hyland, Y.-C. Lau, C.-J. Li, R.S. Lima, A. McDonald, (September 27-29, 2011 (Hamburg, Germany)), Springer, n.d., pp. 421–426.
33. G. Bolelli, J. Rauch, V. Cannillo, A. Killinger, L. Lusvardi, and R. Gadow, Microstructural and Tribological Investigation of High-Velocity Suspension Flame Sprayed (HVSFS) Al₂O₃ Coatings, *J. Therm. Spray Technol.*, 2009, **18**(1), p 35-49
34. S. Goel, S. Björklund, N. Curry, U. Wiklund, and S. Joshi, Axial Suspension Plasma Spraying of Al₂O₃ Coatings for Superior Tribological Properties, *Surf. Coat. Technol.*, 2017, **315**, p 80-87
35. M. Li and P.D. Christofides, Computational Study of Particle In-Flight Behavior in the HVOF Thermal Spray Process, *Chem. Eng. Sci.*, 2006, **61**(19), p 6540-6552
36. B. Samareh and A. Dolatabadi, A Three-Dimensional Analysis of the Cold Spray Process: The Effects of Substrate Location and Shape, *J. Therm. Spray Technol.*, 2007, **16**(5–6), p 634-642
37. T. Varis, T. Suhonen, A. Ghabchi, A. Valarezo, S. Sampath, X. Liu, and S.P. Hannula, Formation Mechanisms, Structure, and Properties of HVOF-Sprayed WC-CoCr Coatings: an Approach toward Process Maps, *J. Therm. Spray Technol.*, 2014, **23**(6), p 1009-1018
38. L. Pawlowski, *The Science and Engineering of Thermal Spray Coatings*, 2nd ed., Wiley, West Sussex, 2008
39. J. Kiilakoski, F. Lukac, H. Koivuluoto, P. Vuoristo, Cavitation Wear Characteristics of Al₂O₃-ZrO₂ -Ceramic Coatings Deposited by APS and HVOF -Processes. in *Proceedings of the ITSC 2017*, (Düsseldorf, Germany), DVS Media GmbH, Düsseldorf, Germany, 2017, pp. 928–933.
40. V. Matikainen, K. Niemi, H. Koivuluoto, and P. Vuoristo, Abrasion Erosion and Cavitation Erosion Wear Properties of Thermally Sprayed Alumina Based Coatings, *Coatings*, 2014, **4**(1), p 18-36
41. V. Matikainen, S. Rubio Peregrina, N. Ojala, H. Koivuluoto, J. Schubert, and P. Vuoristo Houdková, Erosion Wear Performance of WC-10Co4Cr and Cr₃C₂-25NiCr Coatings Sprayed with High-Velocity Thermal Spray Processes, *Surf. Coat. Technol.*, 2019, **370**, p 196-212

Publisher's Note Springer Nature remains neutral with regard to jurisdictional claims in published maps and institutional affiliations.